Assessment of missile hazards: Evaluation of the fragment number and drag factors

Gianfilippo Gubinelli [a], Valerio Cozzani [b],*

[a] Dipartimento di Ingegneria Chimica, Chimica Industriale e Scienza dei Materiali, Università degli Studi di Pisa, via Diotisalvi n.2, 56126 Pisa, Italy
[b] Dipartimento di Ingegneria Chimica, Mineraria e delle Tecnologie Ambientali, Alma Mater Studiorum - Università di Bologna, via Terracini n.28, 40131 Bologna, Italy

ARTICLE INFO

ABSTRACT

An approach was proposed for the assessment of the expected number and drag factor of fragments generated in the collapse of a vessel due to internal pressure. The analysis of a database reporting data on more than 140 vessel fragmentation events allowed the identification of a limited number of fragment reference shapes. The correlation of fragment reference shapes to the vessel credible fragmentation patterns allowed the assessment of the expected number and reference shape of fragments generated. Starting from the fragment reference shapes identified, simplified functions for drag factor calculation were developed, based on few geometrical parameters of the vessel undergoing the fragmentation event. The probabilistic models for the expected shape and number of fragments generated and the simplified drag factor functions developed may constitute an important input for the analysis of the possible fragment trajectories in the framework of missile hazard assessment.

© 2008 Elsevier B.V. All rights reserved.

1. Introduction

Accidental scenarios involving the catastrophic failure of vessels may result in the projection of fragments at relevant distances [1–9]. In several industrial accidents, fragment projection was recorded as the cause of fatalities, injuries and of damage to process equipment [1,2,10]. A particular concern related to fragment projection comes from the possibility of triggering domino events. Since projection distances may be very high, projected fragments are capable of generating secondary accidents at relevant distances from the primary scenario. Safety distance criteria may hardly be applied to prevent escalation events (domino accidents) triggered by fragment projection [6,11,12]. Therefore, the use of quantitative risk analysis (QRA) may be effective to manage the risk of domino accidents triggered by fragment projection [13–15]. However, a well-accepted and validated comprehensive approach to the quantitative assessment of risk caused by fragment projection still needs to be defined. Several simplified procedures were proposed, based on a direct statistic analysis of post-accident data [7,16].

The fundamental approach to fragment trajectory analysis proposed by Baker et al. [10] was used to develop comprehensive ballistic methodologies for the calculation of the impact probabilities of a fragment [17–20]. These more advanced models, however,

need the probabilistic assessment of the initial projection parameters. Previous studies on this issue were mainly oriented to the analysis of the fragmentation of LPG pressurised vessels due to fired BLEVEs [7,8,20,21]. More recently, the concept of "fragmentation pattern", first introduced by Holden and Westin [7,8,21,22], was revisited and used for the analysis of an extended set of accidental events [23]. The results suggested the presence of preferential fragmentation modes, dependent on the accidental scenario and the vessel shape. A limited set of credible fragmentation patterns was identified.

In the present study, a database including detailed data on more than 140 vessel fragmentation accidents was used to investigate the shapes, the expected number, and the drag factors of fragments. The data on the geometries of fragments generated in past accidental events allowed the identification of a limited set of "ideal" reference shapes. The analysis of the reference fragment shapes was used to develop simplified drag factor functions to be used in the assessment of expected fragment flight distance and trajectory using the approach developed by Baker et al. [10]. The available data also allowed the development of a simplified probabilistic approach to the assessment of the expected number of fragments generated in a fragmentation event. Probability distribution functions were obtained for the number of fragments and for the corresponding drag factor as a function of vessel fragmentation pattern.

It is worth mentioning that the present study was carried out within a more general research project, aiming to the development of a comprehensive and systematic methodology for the

* Corresponding author. Tel.: +39 051 2090240; fax: +39 051 2090247.
E-mail address: valerio.cozzani@unibo.it (V. Cozzani).

Nomenclature

a	dimensional constant ($kg\,m^{-3}$)
A_D	section of the fragment on a plane perpendicular to fragment trajectory (m^2)
b	dimensional constant (m^{-1})
C_D	drag coefficient, function of the fragment shape and of its orientation with respect to the flow direction ($kg\,m^{-2}$)
CE	cylinder (model shape in Table 2)
CR	cone roof (model shape in Table 2)
D	target distance from the fragment source point (m)
DF	fragment drag factor as defined by Baker et al. [10]
k	fragment drag factor (m^{-1})
l	length (see Table 2) (m)
l_1	length (see Table 2) (m)
M	fragment weight (kg)
N	number of fragments
PL	plate (model shape in Table 2)
PT	tube section (model shape in Table 2)
PTE1	tube-end section—reference 1 (model shape in Table 2)
PTE2	tube-end section—reference 2 (model shape in Table 2)
r	radius (see Table 2) (m)
SC	spherical cap (model shape in Table 2)
u	initial fragment projection velocity ($kg\,s^{-1}$)
V	vessel volume (m^3)

Greek symbols

α_i	sensitivity index
α_{lim}	threshold value for the sensitivity index α_i
χ	ratio between the maximum and the minimum drag factors of the fragments due to the variation of a single geometrical parameter selected from those used to define the fragments shape (Eq. (6))
γ	spherical cap angle (see Table 2)
ω	weight factor in drag factor functions
ξ	tube-end angle (see Table 2)
ψ	tube-end angle (see Table 2)

quantitative assessment of fragment damage probability in the framework of quantitative risk analysis and of domino effect assessment [11,19,24].

2. Fragment reference shapes

2.1. Fragmentation patterns

Several simplified approaches were proposed in the literature to estimate the number and shape of fragments generated in the catastrophic failure of a vessel (e.g. see [1,9,10,25–28] and references cited therein). The assessment of the expected number of fragments formed in the failure of a vessel may be approached by the analysis of likely reference fragmentation patterns, that may be defined for different vessel categories. The concept of fragmentation patterns was introduced by Holden and Westin to analyze the shape of fragments formed in the BLEVEs of horizontal cylindrical pressurized vessels [8,21]. In a previous study, this approach was extended to other vessel shapes and explosion scenarios, and a limited number of likely fragmentation patterns were identified from the analysis of more than 140 vessel fragmentation events [23]. Fig. 1 summarizes the main features of the credible fragmen-

tation patterns identified. Fragmentation patterns are determined by the fracture mechanism, that in turn is influenced by the material toughness. Vessel wall temperature and transient loads due to internal pressure are the main factors that determine the fracture propagation mechanism. It is widely recognized that ductile fractures resulting in a limited number of fragments are expected to be the prevailing fragmentation mechanism in BLEVEs and in physical explosions [26–28]. On the other hand, in the case of confined explosions and of runaway reactions, brittle fracture resulting in a high number of fragments may be expected, although brittle-ductile transition is possible for high toughness vessels. A strong correlation thus exists among the vessel type, the scenario causing vessel fragmentation and the fragmentation pattern experienced by the vessel [23,27]. Table 1 shows the results of the analysis of the available data on past accidents. A clear correspondence is present between the vessel type and the primary scenario causing the vessel collapse, as well as between the likely fragmentation pattern and the explosion scenario.

2.2. Fragment reference shapes

The analysis of vessel fragmentation patterns may give important information on the expected shape of the fragments generated. The expected fragment shape is of fundamental importance in order to estimate the fragment drag factor, that is needed to assess the projection distance of the fragments [19].
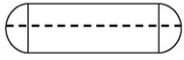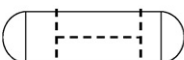
As shown in Fig. 1, the different fragmentation patterns result in the detachment and projection of different parts of the vessels undergoing fragmentation. The vessel fragmentation process obviously results in fragments having irregular shapes, as shown in Fig. 2. However, on the basis of the actual fragment shapes and having in mind the original shape of equipment parts that originated the fragments, it was possible to define a few reference model shapes for the fr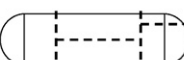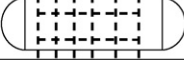agments. These reference shapes may be used to represent the actual fragment shapes, at least in the framework of the estimation of the fragment drag factor.

A systematic analysis of an extended database reporting details on more than 140 fragmentation events was thus undertaken. The results allowed the identification of the fragment reference shapes reported in Table 2. The comparison of Table 2 with Fig. 2 gives an example of the clear correspondence that may be found between the actual fragment shapes and the reference shapes considered in the present analysis.

A further element coming from the analysis of the database is the evident correlation among the fragmentation pattern of the vessel and the reference shapes of the fragments formed. Fig. 1 shows that well defined fragment reference shapes may be associated to each fragmentation pattern.

3. Expected number of fragments

Table 3 reports the expected and the observed ranges of fragment number for the fragmentation patterns considered in the present study. The observed ranges of fragment number were derived from the analysis of 143 fragmentation events reported in the database developed within the present study [22]. The results of the analysis evidenced that the number of fragments is strictly dependent on the vessel fragmentation pattern, as shown in Table 3. Well defined ranges of values may be associated to the expected number of fragments for each likely reference fragmentation pattern. As shown in Fig. 1, several reference fragmentation patterns lead to the formation of a fixed number of fragments (this is the case of FPs CV1, CV2, CV3, CV4, CV7, CV11, and CR1). On the other hand, a few more complex patterns may lead to the formation of a vari-

ID	Fragmentation pattern	Expected fragment reference shapes	Number of fragments
CV1		An axial fracture starts and propagates in two opposite directions. If the two tips do not meet (more probable), 1 fragment (the entire vessel) may be projected, but no detached piece is formed. The equipment may not be deformed thus giving a CE fragment or may be flattened, thus giving a PL fragment.	1 (CE or PL)
CV2		The fracture, likely to start in the axial direction, may propagate in the circumferential direction thus generating two tube-ends (PTE2). If the axial crack propagates on the tube-end and stops, a flattened tube-end may be generated (PL), thus one tube end may become a plate.	1 (PTE2) 1 (PTE2 or PL)
CV3		Similar to CV2, but one entire tube-end is projected while the other tube-end is separated in 2 fragments	1 (PTE2, $\psi=0$) 1 (PTE2, $\psi>0$) 1 (PTE1)
CV4		Similar to CV2, but one entire tube-end is projected while the other tube-end is separated in 3 fragments, one of which is generally flattened	1 (PTE2, $\psi=0$) 1 (PL) 2 (PTE1)
CV7		An axial crack may propagate in circumferential direction in zones where a stress concentration (thickness change, supports, pipe connections), defects or weldings are present. It is highly probable that the circumferential cracks are located at the ends. The shell fragment is generally flattened during the flight	2 (PTE2, $\psi=0$) 1 (PL)
CV11		Similar to CV7, but one entire tube-end is projected while the other tube-end is separated in 2 fragments	1 (PTE2, $\psi=0$) 1 (PTE2, $\psi>0$) 1 (PL) 1 (PTE1)
CV21		Similar to CV7, but the shell is separated in more than one fragment.	2 (PTE2, $\psi=0$) >3 (PL or PT)
SV1		A fracture on a spherical vessels may propagate in all directions since it will be always subjected to the same stress. It is possible to have more than one point of failure. The number of fragments tends to grow with the vessel volume (higher the volume of the sphere higher the surface area) because there is a higher probability for the fracture to undergo conditions for branching	>1 (SC)
CR1		The cone roof is projected	1 (CR)
SEE	Sharp-edged Equipment	Fractures along the edges	>1 (PL)

Fig. 1. Expected fragment reference shapes and expected number of fragments for credible vessel fragmentation patterns (fragment reference shapes: CE: cylinder; SC: spherical cap; CR: cone roof; PL: plate; PT: tube section; PTE1: tube-end section 1; PTE2: tube-end section 2; see Table 2 for reference shape definitions).

able number of fragments (FPs CV21 and SV1). The considerable agreement present in Table 3 among the expected and observed ranges of fragments formed thus allowed the use of observational data to obtain indications on the expected number and shape of fragments. Table 3 summarizes the expected number of fragments for each fragmentation pattern, and, where needed, the probability distributions of fragment number, validated using the available data on past accidents.

For cylindrical vessels, the only fragmentation pattern that leads to a variable number of fragments is CV21 (see Fig. 1), for which a number of fragments comprised between 5 and 9 was observed, as shown in Table 3. A uniform probability of distribution well represented the observed data on past accidents.

In the case of fragmentation patterns CV1, CV2, and CV21, a fixed number of fragments is expected but the reference shape of fragments may be different (see Fig. 1). The overall number of fragments for each of the different reference shape was thus estimated on the basis of observational data and is reported in Table 4.

In the case of spherical vessels, a rough correlation is present among vessel volume and the number of fragments generated,

since a higher probability for fracture branching corresponds to higher vessel volumes and higher vessel surface areas. The more extended data set available allowed an updating of the linear correlation originally proposed by Holden and Reeves [7]. The correlation obtained in the present approach, reported in Table 3, gives more reasonable results for low vessel volumes (number of fragments approaches zero for volumes near to zero). Nevertheless, as shown in Fig. 3, the scarce data available result in a relevant uncertainty of the correlation, that may easily result in errors up to a factor 2. However, due to its simplicity, the proposed correlation is attractive for a preliminary estimation of the expected number of fragments in the framework of quantitative risk analysis.

4. Drag factor functions for fragment reference shapes

4.1. Development of drag factor functions

The estimation of the expected number of fragments and of fragment reference shapes is a first step towards the calculation of possible fragment trajectories, that should be assessed to esti-

Table 1

Categories of primary scenarios leading to vessel fragmentation: number of events recorded with respect to vessel type and observed probabilities (%) of credible fragmentation patterns
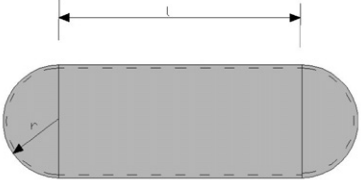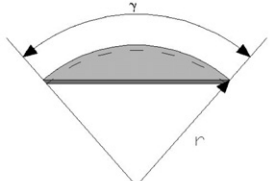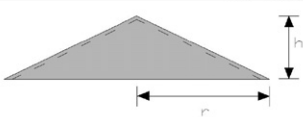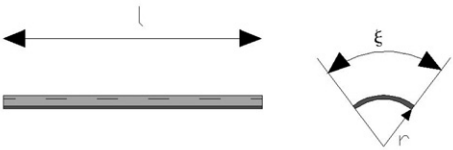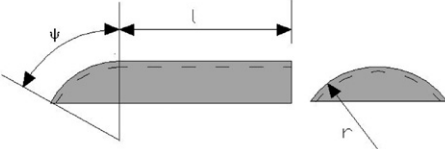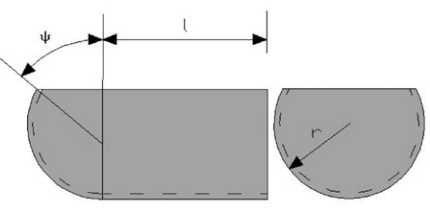
	Id	BLEVE (F)	PE, BLEVE (NF)	CEx	RR	Total
Type of vessel						
Atmospheric vessel (any)	AV	0	0	4	12	16
Horizontal cylindrical pressurized vessel	HCV	100	19	8	0	127
Vertical cylindrical pressurized vessel	VCV	5	1	5	6	17
Spherical pressurized vessel	SV	11	2	0	0	13
Fragmentation pattern						
	CV1	6	0	0	29	5
	CV2	55	67	90	43	60
	CV3	11	8	0	0	9
	CV4	0	13	0	0	2
	CV7	28	8	0	14	21
	CV11	0	4	0	0	1
	CV21	0	0	10	14	2
	SV1	100	100	0	0	100
	CR1	0	0	100	0	100
Sharp-edged equipment (fractures along the edges)	SEE	0	100	100	0	100

BLEVE: Boiling liquid expanding vapor explosion; F: fired; NF: non-fired; PE: physical explosion; CEx: confined explosion; RR: runaway reaction.
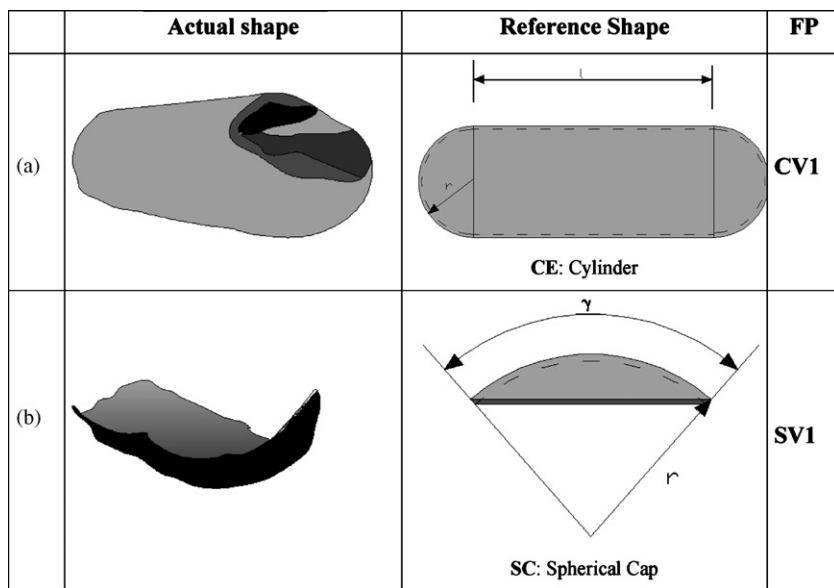
Fig. 2. Examples of actual fragment shapes. (a) Tube-end fragment projected in the accident of San Juan de Ixhuatepec (Mexico City, Mexico), November 19th 1984 [29]. (b) Spherical cap fragment projected in the accident of Albert City (Iowa, U.S.A.), April 9th 1998 [30].

Table 2
Reference shapes defined for the analysis of fragment drag factors

| **CE: CYLINDER**	
	projection of the entire equipment (in the case of horizontal or vertical cylindrical vessels)
Parameters: wall thickness, t; density, ρ; l and r as shown in the figure	
SC: SPHERICAL CAP	
	reference shape assumed for fragments generated in the rupture of a spherical vessel if the number of fragment is higher than 4.
Parameters: wall thickness, t; density, ρ; r and γ as shown in the figure	
CR: CONE ROOF	
	roof of an atmospheric tank (fragment generated by the propagation of a crack along the connection with the cylindrical shell).
Parameters: wall thickness, t; density, ρ; r and h as shown in the figure	
PL: PLATE	
	flattened shell or pipe section end, or section of a sharp-edged atmospheric equipment.
Parameters: wall thickness, t; density, ρ; l and l_1 as shown in the figure	
PT: TUBE SECTION	
	Fragment of a cylindrical shell, generated by the propagation of two circumferential cracks and of one or two axial cracks. In the first case the fragment results from the flattening of a cylindrical shell of smaller radius. If ξ = 2 π: tube, fragment of a cylindrical shell generated by the propagation of two circumferential cracks.
Parameters: wall thickness, t; density, ρ; r, l and ξ as shown in the figure	
PTE1: TUBE END SECTION – reference 1	
	fragment of a cylindrical shell, generated by the propagation of a circumferential and of an axial crack
Parameters: wall thickness, t; density, ρ; r, l and ψ as shown in the figure	
PTE2: TUBE END SECTION - reference 2	
	Fragment of a cylindrical shell, generated by the propagation of a circumferential and of an axial crack. If ψ=0: tube end, fragment of the shell of a cylindrical vessel, generated by the propagation of a circumferential crack.
Parameters: wall thickness, t; density, ρ; r, l and ψ as shown in the figure	

Table 3
Observed and expected range of the number of fragments formed in each vessel fragmentation pattern

FP	Expected fragment number	Range of observed number of fragments	Probabilistic models introduced for fragment number (N)
CV1	1	1	$N = 1$
CV2	2	2	$N = 2$
CV3	3	3	$N = 3$
CV4	>3	4	$N = 4$
CV7	3	3	$N = 3$
CV11	4	4	$N = 4$
CV21	>4	5–9	Uniform pdf for $5 \leq N \leq 9$
SV1	>1	3–19	$N = -0.425 + 6.115 \, 10^{-3} \, V$
CR1	1	1	$N = 1$

Probability distributions for fragment number were obtained from observational data. See Table 2 for symbol definition.

mate the probability of fragment impact on a secondary target. The method proposed by Baker et al. [10] is among those more widely used for the calculation of the trajectory of projected fragments. As shown in a previous study [19], the method is also suitable to assess the impact probability of projected fragments. However, one of the main difficulties in the use of the approach of Baker et al. [10] in a risk assessment framework is the prediction of the drag factor of the fragments. As a matter of fact, the calculation of a drag constant k is needed to assess fragment trajectories by this approach [10].
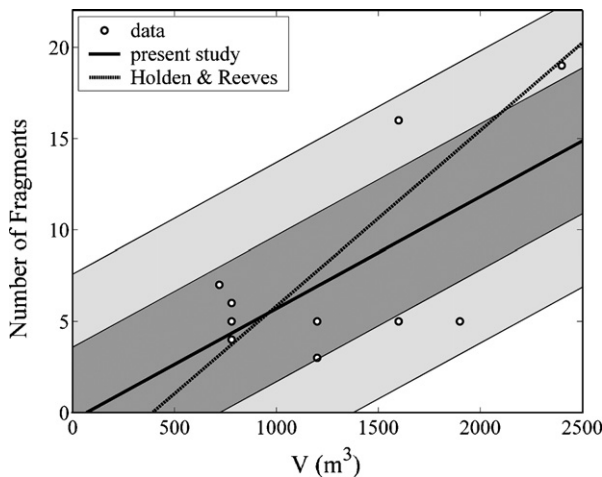
Fig. 3. Comparison of the correlation obtained in the present study for the number of fragments generated in the rupture of spherical vessels ($N = -0.425 + 6.115 \times 10^{-3} \, V$) with available data on past accidents. The correlation of Holden and Reeves [7] is also reported ($NF = -3.77 + 0.96 \times 10^{-2} \, V$). V: Vessels volume in m³. Heavy grey region: less than one standard deviation ($\sigma_N = 4$) with respect to the correlation. Light grey region: less than two standard deviations with respect to the correlation.

The following general expression may be used for the calculation of the drag constant [19]:

$$k(\bar{x}) = a \cdot \text{DF}(\bar{x}) + b \tag{1}$$

where a and b are dimensional constants, DF is the fragment drag factor, and the set of geometrical parameters used to define the fragment is expressed as follows:

$$\bar{x} = [x_1, \dots, x_n] \tag{2}$$

For chunky fragments, the fragment drag factor may be estimated as follows [10]:

$$\text{DF} = \frac{C_D A_D}{M} \tag{3}$$

where C_D is a drag coefficient, function of the fragment shape and of its orientation with respect to the flow direction, A_D is the section of the fragment on a plane perpendicular to the trajectory, and M is the mass of the fragment. Since the orientation of the fragment with respect to the trajectory is usually unknown when possible fragmentation accidents are assessed, an average value of DF may be used in Eq. (3):

$$\text{DF}_a = \frac{\text{DF}_{max} + \text{DF}_{min}}{2} \tag{4}$$

where DF_{min} and DF_{max} are, respectively, the minimum and the maximum values of DF that may be obtained considering all the possible orientations of the fragment with respect to the flight trajectory. In a previous study [19] it was shown that this approach is acceptable since the errors deriving from this assumption in the estimation of the drag factor are unlikely to cause relevant errors in the values of the impact probability.

As discussed above, the fragment drag factors depend on fragment shape, but also on fragment size and weight. The latter two factors are dependent on the actual geometrical sizes of the vessel that undergoes fragmentation and on the actual position of the cracks formed. Thus, the calculation of the drag factors of fragments that may be generated requires to take into account all these elements. The reference shapes defined in Table 2 made possible the description of the fragment shapes using a limited number of geometrical parameters. This allowed the development of simple analytical functions for the evaluation of the fragment drag factors, reported in Appendix A.

4.2. Identification of the critical parameters of the drag factor functions

The drag factor functions include several parameters that may vary depending on the actual fragmentation accident and on the geometry of the vessel undergoing the fragmentation and that are unknown "a priori". However, only some of these parameters are likely to have a non-negligible influence on the final values of the drag factor. The identification of these critical parameters

Table 4
Number of fragments for the different reference shapes of each vessel fragmentation pattern

FP	CE	SC	CR	PL	PT	PTE1	PTE2
CV1	0.5	–	–	0.5	–	–	–
CV2	–	–	–	0.72	–	–	1.28
CV3	–	–	–	–	–	1	2
CV4	–	–	–	1	–	2	1
CV7	–	–	–	1	–	–	2
CV11	–	–	–	1	–	1	2
CV21	–	–	–	–	0.5 (NF-2)	0.5 (NF-2)	2
SV1	–	See Table 3	–	–	–	–	–
CR1	–	–	1	–	–	–	–

See Table 2 for symbol definition.

Table 5
Credible intervals and reference values assumed for the parameter of the drag factor functions

k functions	Parameters								Mass ranges	
	l (m)	l_1 (m)	r (m)	h (m)	γ (rad)	ξ (rad)	ψ (rad)	t (m)	M_{min} (kg)	M_{max} (kg)
k_{CE}	1–20		1–5					0.01–0.05	1400	370,000
k_{SC}					0.2π–π			0.01–0.05	50	120,000
k_{CR}			1.5–20	0.25–3.5				0.005–0.01	300	96,000
k_{PL}	1–10	1-10						0.005–0.05	40	40,000
k_{PT}	1–10		1–5			0–2π		0.005–0.05	5	120,000
k_{PTE1}	1–10		1–5				0–$(\pi/2)$	0.005–0.05	5	92,000
k_{PTE2}	1–10		1–5				0–$(\pi/2)$	0.005–0.05	245	184,000

Table 6
Sensitivity index α_i estimated for each parameter and each fragment shape calculated assuming a material density of 7800 kg/m^3

k functions	Range	Parameters							
		l (m)	l_1 (m)	r (m)	h (m)	γ (rad)	ξ (rad)	ψ (rad)	t (m)
k_{CE}	1.9×10^{-4} to 1.6×10^{-3}	1.4	–	1.2	–	–	–	–	11.6
k_{SC}	5×10^{-4} to 4.5×10^{-3}	–	–	–	–	1.4[a]	–	–	10.5
k_{CR}	2×10^{-3} to 1.1×10^{-2}	–	–	2.8	2.8	–	–	–	2.0
k_{PL}	1×10^{-3} to 9×10^{-3}	1.1	1.1	–	–	–	–	–	10.2
k_{PT}	4×10^{-4} to 1×10^{-2}	1.3	–	1.0	–	–	3	–	10.6
k_{PTE1}	4×10^{-4} to 1×10^{-2}	1.3	–	1.2	–	–	–	2.2	10.3
k_{PTE2}	3×10^{-4} to 5×10^{-3}	1.5	–	1.5	–	–	–	1.2	12.3

[a] 1.1 for $\gamma < 0.7\pi$.

is an important step to simplify the drag factor functions in the framework of fragment impact probability assessment. A sensitivity analysis was thus performed on the drag factor functions. Considering the general expression for the drag factor constant given by Eq. (1), for each of the x_i parameters needed for the calculation of the drag factor it is possible to identify a range of credible values of the parameter, ΔX_i:

$$x_i \in \Delta X_i, \quad \text{for } i = 1, \ldots, n \tag{5}$$

By conservative assumptions based on the analysis of the design characteristics of the different types of vessels used in chemical and process plants, the maximum credible range of each parameter was determined for the more relevant categories of process vessels (horizontal cylindrical pressurized vessels, cone roof atmospheric vessels, columns).

Table 5 reports the parameters considered in the sensitivity analysis. Vessel material density, influencing fragment weight but not fragment surface, does not appear in the table since it was directly assumed as a critical parameter. Table 5 also reports the range considered in the analysis for each parameter. Using these ranges it was possible to evaluate the ratio χ of the maximum over the minimum value of the drag factor function k obtained for the variation of the x_i parameter in the interval ΔX_i, assuming for the other parameters constant reference values, X_j:

$$\chi^{i,\bar{j}} = \frac{\max_{x_i}(k(x_i, \bar{j}))}{\min_{x_i}(k(x_i, \bar{j}))}, \tag{6}$$

where:

$$\bar{j} = [x_1 = X_1, \ldots, x_{i-1} = X_{i-1}, x_{i+1} = X_{i+1}, \ldots, x_n = X_n] \tag{7}$$

A sensitivity index α_i was introduced to assess the influence of the parameter x_i on the function k. This was defined as the maximum value of χ that may be obtained for all the possible vectors $\bar{j}$:

$$\alpha_i = \max_{\bar{j}}(\chi^{i,\bar{j}}) \tag{8}$$

A high value of α_i thus indicates a high influence of the parameter x_i on the function k. Table 6 reports the values of the

sensitivity index calculated for each parameter on the basis of Table 5.

The above defined sensitivity parameter was compared to that of a threshold value to understand the influence of each parameter on the value of the drag factor. The model for fragment impact probability proposed by Gubinelli et al. [19] allows the calculation of the impact probability of a fragment on a defined target as a function of the initial projection velocity (u), of the fragment drag factor (k), and of the distance (D) of the target from the position of the fragment source:

$$P_{imp} = P_{imp}(u, k, D) \tag{10}$$

The sensitivity threshold value, α_{lim}, was thus identified using the impact probability model [19]. A conservative range of velocities (50–300 m/s), drag factor values (10^{-4} to 10^{-2}), and target distances (15–3000 m) was considered in the analysis [19]. Different target geometries were considered. Several geometrical series were defined for the k values ($k_i = k_{i-1}\theta$, with θ parameter of the series) within the assumed drag factor range. For each k_i series, the maximum absolute difference (MAD) and the maximum relative difference (MRD) of the probability of impact estimated considering all the adjacent k values (k_{i-1}, k_i) within each series were calculated.

A sensitivity threshold value, α_{lim}, was defined as the higher θ value for which MAD resulted below 1×10^{-3} and MRD lower than 50%. Thus, a variation of the drag factor k yielding a value α_i lower than the sensitivity threshold, α_{lim} results in a maximum absolute difference of the probability of impact always lower than 1×10^{-3} and in a maximum relative difference always lower than 50%. It must be recalled that Gubinelli et al. [19] found that the maximum credible values for the probability of impact of a single fragment are of about 2×10^{-1} for realistic geometries. Thus, the above selection of the threshold value α_{lim} seems compatible with the usual uncertainty associated in a QRA framework. On the basis of the ranges considered for the drag factors, the fragment velocities and the target distances, a value of 1.6 was calculated for α_{lim}.

The comparison of the α_i value calculated for each parameter of the drag factor functions (see Table 6) with the threshold value α_{lim} allowed the identification of the critical parameters of the drag

Table 7
Critical parameters identified in drag factor functions

Drag factor functions	Critical parameters	Reference values for non-critical parameter
CE	t, ρ	$l = 10; r = 2.5$
SC	t, ρ	$\gamma = 0.6\pi$
CR	r, h, t, ρ	–
PL	t, ρ	$l = 5; l_1 = 5$
PT	ξ, t, ρ	$l = 5; r = 2.5$
PTE1	ψ, t, ρ	$l = 5; r = 2.5$
PTE2	t, ρ	$l = 5; r = 2.5; \psi = \pi/4$

factor functions that verify the condition $\alpha_i \geq \alpha_{\lim}$. Table 7 reports the critical parameters identified by this procedure for each drag factor function associated to a fragment reference shape. As stated above, vessel material density was directly assumed as a critical parameter in the analysis.

Table 7 also reports the reference values assumed for the non-critical parameters. In the following, a constant value was considered for these parameters, equal to the mean value in the credible range considered in the analysis (see Table 5). It is important to remark that, in analogy with material density, the fragment thickness always resulted a critical parameter in the evaluation of the drag factor. The reason for this lies in the fact that, as in the case of material density, the thickness heavily influences the fragment mass, but not the surface of the fragment exposed to the drag forces (see Eq. (3)). A second important observation coming from Table 7 is that the results obtained evidence that only in the case of the fragments formed from cone roof projection it is necessary to know all the geometrical parameters of the fragment in order to calculate the drag factor. For all the other fragment shapes, the influence of some parameters could be neglected. This is due to the fact that the variation of these parameters has an almost equal influence on the fragment mass and on the surface area exposed to drag forces, so that the two effects balance each other in the final value obtained for the drag factor (see Eq. (3)).

4.3. Simplified drag factor functions

The identification of the critical parameters made possible the simplification of the drag factor functions. Revised drag factor func-

tions were developed and are presented in Table 8. In the simplified revised functions, only the critical parameters listed in Table 7 are present, while the constant reference values reported in the table were assumed for the non-critical parameters.

With few exceptions, the simplified drag factor functions allow the calculation of the fragment drag factor only on the basis of the wall thickness and the material density of the vessel undergoing the fragmentation. In the case of cone roof shaped fragments, Table 7 evidences that all the geometrical parameters of the roof are necessary to evaluate the drag factor. Thus, in this case the knowledge of the design details of the vessel undergoing fragmentation is needed to estimate the drag factor. On the other hand, as shown in Table 8, the drag factor functions obtained for tube sections and for tube ends (1) still show a dependence on the ξ and ψ angles (see Table 2), as the sensitivity threshold $\alpha_{\lim}$, was exceeded for both these parameters. Since the value of these parameters is unknown and is not predictable "a priori", a further simplification was introduced to allow the use of these drag factor functions. The values of the sensitivity parameter α_i is strictly influenced by the credible ranges chosen for each parameter. If the credible range of a given parameter is reduced, it is possible to neglect the influence of the parameter on the value of the drag factor. Therefore, as shown in Table 8 a discrete distribution of the values of ξ and ψ was introduced, and different simplified drag factor functions were obtained for each value considered. A uniform probability distribution was assumed for each of the values considered, in coherence with the results coming from past accident analysis that did not evidence any preferential value of these angles.

5. Assessment of expected number and drag factor of projected fragments

In the framework of probabilistic risk analysis, the approach developed for the assessment of the number and drag factor of fragments allows the estimation of the expected values of these parameters in a vessel fragmentation event. It is worth to recall that these are important input parameters in the analysis of fragment trajectories aimed to the assessment of possible damage caused by projected fragments.

As shown in Table 1, on the basis of past accident data analysis it is possible to identify the credible fragmentation patterns and their expected frequency, $f(FP_i)$. The approach developed

Table 8
Simplified drag factor functions for the evaluation of fragment impact probability

k'' function[a]	K value range	Parameters	Proposed simplified function[b]	
k''_{CE}	1.9×10^{-4}–1.6×10^{-3}	ρ, t	$DF''_{CE} = \frac{0.166}{\rho t}$	
k''_{SC}	5×10^{-4}–4.5×10^{-3}	ρ, t	$DF''_{SC} = \frac{0.460}{\rho t}$	
k''_{CR}	$2 \times 10^{-4}, 1.1 \times 10^{-2}$	r, h, t, ρ	$DF''_{CR} = DF_{CR}(r, h, t)$	
k''_{PL}	1×10^{-3}–9×10^{-3}	ρ, t	$DF''_{PL} = \frac{1.17 + 0.41t}{\rho t}$	
k''_{PT}	4×10^{-4}–1×10^{-2}	ξ, t, ρ	$\xi = \pi/2$	$DF''_{PT} = \frac{1}{\rho t}\left(\frac{2.701}{5-t} + 0.205t\right)$
			$\xi = \pi$	$DF''_{PT} = \frac{1}{\rho t}\left(\frac{1.910}{5-t} + 0.205t\right)$
			$\xi = 3\pi/2$	$DF''_{PT} = \frac{1}{\rho t}\left(\frac{1.273}{5-t} + 0.205t\right)$
			$\xi = 2\pi$	$DF''_{PT} = \frac{1}{\rho t}\left(\frac{0.955}{5-t} + 0.205t\right)$
k''_{PTE1}	4×10^{-4}–1×10^{-2}	ψ, t, ρ	$\psi = \pi/8$	$DF''_{PTE1} = \frac{0.550}{\rho t}$
			$\psi = \pi/4$	$DF''_{PTE1} = \frac{0.450}{\rho t}$
			$\psi = 3\pi/8$	$DF''_{PTE1} = \frac{0.440}{\rho t}$
			$\psi = \pi/2$	$DF''_{PTE1} = \frac{0.350}{\rho t}$
k''_{PTE2}	3×10^{-4}–5×10^{-3}	t, ρ		$DF''_{PTE2} = \frac{0.240}{\rho t}$

[a] In this case $k'' = 0.69$ and $DF'' - 3.28 \times 10^{-5}$.
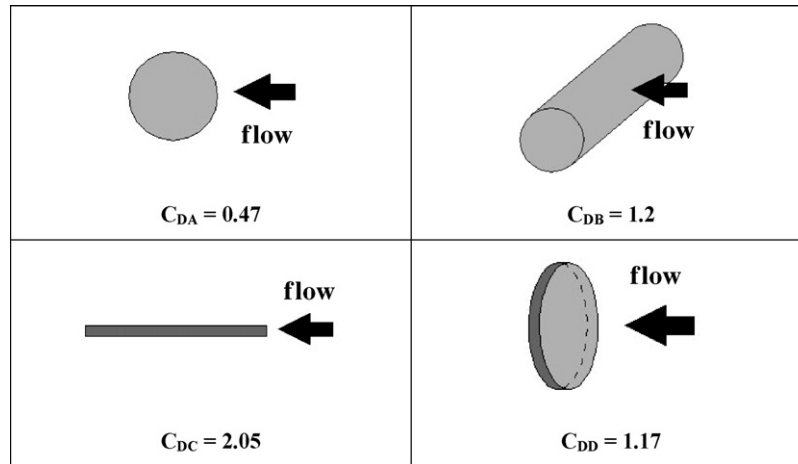[b] DF'' are the simplified functions.

Fig. 4. Drag factor coefficients (from Baker et al. [10]).

allows the identification of the expected fragment reference shapes and the assessment of the expected fragment number (see Tables 2 and 3 and Fig. 1). These data may be used to esti-mate a minimum and maximum expected number of fragments, as well as the expected probability of obtaining a given num-ber of fragments in a vessel fragmentation accident. Moreover, a simplified approach to fragment drag factor calculation may be

associated to each fragmentation pattern (see Table 8). Table 9 summarizes the models and reports the probability values that should be used for the combination of the drag factor functions in Table 8.
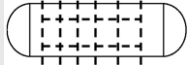
The data in Table 9 are an important input for a more sound analysis of the hazards deriving from vessel fragmentation events. The results of this procedure allow the characterization of a frag-

Table 9
Correlation between FPs (see Table 1), fragments shapes, simplified drag factor (k'') functions and weight factors (ω)

FP	Total number fragments	Reference shape	Conditional probability ω	Number of fragments	Simplified drag factor function
CV1	1	CE	0.5	1	k''_{CE}
		PL	0.5	1	k''_{PL}
CV2	2	PTE2	1	1	k''_{PTE2}
		PTE2	0.28	1	k''_{PTE2}
		PL	0.72	1	k''_{PL}
CV3	3	PTE2	1	2	k''_{PTE2}
		PTE2	1		
		PTE1	0.25	1	$k''_{PTE1}\ (\psi = \pi/8)$
			0.25		$k''_{PTE1}\ (\psi = \pi/4)$
			0.25		$k''_{PTE1}\ (\psi = 3\pi/8)$
			0.25		$k''_{PTE1}\ (\psi = \pi/2)$
CV4	4	PTE2	1	1	k''_{PTE2}
		PTE1	0.25	2	$k''_{PTE1}\ (\psi = \pi/8)$
			0.25		$k''_{PTE1}\ (\psi = \pi/4)$
			0.25		$k''_{PTE1}\ (\psi = 3\pi/8)$
			0.25		$k''_{PTE1}\ (\psi = \pi/2)$
		PL	1	1	k''_{PL}
CV7	3	PTE2	1	2	k''_{PTE2}
		PL	1	1	k''_{PL}
CV11	4	PTE2	1	2	k''_{PTE2}
		PTE2	1		
		PTE1	0.25	1	$k''_{PTE1}\ (\psi = \pi/8)$
			0.25		$k''_{PTE1}\ (\psi = \pi/4)$
			0.25		$k''_{PTE1}\ (\psi = 3\pi/8)$
			0.25		$k''_{PTE1}\ (\psi = \pi/2)$
		PL	1	1	k''_{PL}
CV21	$5 \leq N \leq 9$	PTE2	1	2	k''_{PTE2}
		PL	0.5	$3 \leq N \leq 7$ unif. pdf(N)	k''_{PL}
		PT	0.125	$3 \leq N \leq 7$ unif. pdf(N)	$k''_{PT}\ (\xi = \pi/2)$
			0.125		$k''_{PT}\ (\xi = \pi)$
			0.125		$k''_{PT}\ (\xi = 3\pi/2)$
			0.125		$k''_{PT}\ (\xi = 2\pi)$
SV1	>1	SC	1	See Table 3	k''_{SC}
CR1	1	CR	1	1	k''_{CR}
SEE	>1	PL	1	Edge number/2	k''_{PL}

Table 10
Results obtained for the fragment reference shape, the number of fragments, the fragment drag factor and the conditional probability of fragment reference shape for the fragmentation of a cylindrical vessel by two alternative fragmentation patterns

Vessel type	Volume (m³)	Diameter (m)	Length (m)	L/D	Thickness (m)	Design pressure (bar)
Cylinder	150	3	18	6	0.018	15

ID	Fragmentation pattern	Reference Shape	Number of fragments	k″	ω
CV2		PTE2	1	1.1×10^{-3}	1
		PTE2	1	1.1×10^{-3}	0.28
		PL	1	5.8×10^{-3}	0.72
CV21		PTE2	2	1.1×10^{-3}	1
		PL	5	5.8×10^{-3}	0.5
		PT		3.8×10^{-3}	0.125
			5	2.7×10^{-3}	0.125
				1.8×10^{-3}	0.125
				1.4×10^{-3}	0.125

Table 11
Results obtained for the fragment reference shape, the number of fragments, the fragment drag factor and the conditional probability of fragment reference shape for the fragmentation of a spherical vessel

Vessel type	Volume (m³)	Diameter (m)	Length (m)	L/D	Thickness (m)	Design Pressure (bar)
Sphere	1600	14.5	–	–	0.072	10

ID	Fragmentation pattern	Reference shape	Number of fragments	k″	ω
SV1		SC	10	2.1×10^{-3}	1

mentation event on the basis of the scenario leading to vessel fragmentation and of few details on the vessel undergoing the fragmentation accident. Tables 10 and 11 show some examples of the results obtained by the application of the procedure, respectively, to a cylindrical and spherical vessels. As shown in the tables, fragment drag factors were calculated for different fragmentation events. In the case of the cylindrical vessel, two different fragmentation patterns were considered. The corresponding fragment number, fragment drag factor and probability fragment shape were easily calculated by the above procedure and are reported in the tables. The data in Tables 10 and 11 may be combined with those in Table 1, concerning the probability of alternative FPs, in order to estimate the overall probability of fragment generation.

6. Conclusions

A general approach based on fragmentation patterns was developed to estimate the expected number of fragments and the fragment drag factors in vessel fragmentation events. The approach was based on the definition of reference fragment shapes, derived from the analysis of available data on fragmentation accidents. Simplified functions were derived for fragment number assessment and for drag factor calculation. The proposed approach provides a route to the assessment of input data required for the characterization of a fragmentation events in the framework of probabilistic risk analysis. The approach yields useful input data for the application of models for fragment trajectory analysis and for fragment impact probability assessment.

Appendix A

The functions in Eqs. (A.1)–(A.7) allow the evaluation of the drag factors for all the fragment model shapes defined in Table 2. The parameters and symbols used in the following equations are defined in Table 2 and in Fig. 4.

$$DF_{CE} = \frac{C_{DA}\pi r + C_{DB}l}{2\pi \rho t(l + 2r)} \tag{A.1}$$

$$DF_{SC} = \frac{C_{DA}}{4\pi \rho t}\left[\frac{\gamma - \sin(\gamma) + 2\pi \sin^2(\gamma/2)}{1 - \cos(\gamma/2)}\right], \quad \gamma < \pi \tag{A.2}$$

$$DF_{CR} = \frac{C_{DC}rh + C_{DD}\pi r^2}{2\pi t \rho(r^2 + h^2)} \tag{A.3}$$

$$DF_{PL} = \frac{C_{DD} + C_{DC}t(\min(l, l_1)/ll_1)}{2t\rho} \tag{A.4}$$

$$DF_{PT} = \begin{cases} \frac{1}{\rho}\left[\frac{C_{DB}r\sin(\xi/2)}{t(\xi/2)(2r - t)} + \frac{C_{DC}}{2l}\right], & \xi \leq \pi \\ \frac{1}{\rho}\left[\frac{C_{DB}r}{t(\xi/2)(2r - t)} + \frac{C_{DC}}{2l}\right], & \xi > \pi \end{cases} \tag{A.5}$$

$$\mathrm{DF_{PTE1}} = \begin{cases} \dfrac{1}{4t\rho}\left[\dfrac{C_{DA}r\left[\pi\sin^2(\psi)+\psi-\sin(\psi)\cos(\psi)\right]+2C_{DB}l\left[2\sin(\psi)+1-\cos(\psi)\right]}{\pi r(1-\cos(\psi))+2l\psi}\right], & \text{if}(1) \\[4mm] \dfrac{1}{4t\rho}\left[\dfrac{C_{DA}r\left[\pi\sin^2(\psi)+2\psi-2\sin(\psi)\cos(\psi)\right]+4C_{DB}l\sin(\psi)}{\pi r(1-\cos(\psi))+2l\psi}\right], & \text{if}(2) \end{cases} \tag{A.6}$$

$$\frac{l}{r} \le \frac{C_{DA}}{2C_{DB}}\left[\frac{\psi-\sin(\psi)\cos(\psi)}{1-\cos(\psi)}\right] \tag{1}$$

$$\frac{l}{r} > \frac{C_{DA}}{2C_{DB}}\left[\frac{\psi-\sin(\psi)\cos(\psi)}{1-\cos(\psi)}\right] \tag{2}$$

$$\mathrm{DF_{PTE2}} = \begin{cases} \dfrac{1}{4t\rho}\left[\dfrac{3C_{DA}r[\pi-\psi+\sin(\psi)\cos(\psi)]+2C_{DB}l[1+\cos(\psi)]}{\pi r[1+\cos(\psi)]+2(\pi-\psi)l}\right], & \text{if}(3) \\[4mm] \dfrac{1}{4t\rho}\left[\dfrac{2C_{DB}l[2+\cos(\psi)]+C_{DA}r[2\pi-\psi+\sin(\psi)\cos(\psi)]}{\pi r[1+\cos(\psi)]+2(\pi-\psi)l}\right], & \text{if}(4) \\[4mm] \dfrac{1}{4t\rho}\left[\dfrac{4C_{DB}l+C_{DA}r[3\pi-2\psi+2\,\sin(\psi))\cos(\psi)]}{\pi r[1+\cos(\psi)]+2(\pi-\psi)l}\right], & \text{if}(5) \end{cases} \tag{A.7}$$

$$\frac{l}{r} \le \frac{C_{DA}}{2C_{DB}}\left[\frac{\pi}{2}-\psi+\sin(\psi)\cos(\psi)\right] \tag{3}$$

$$\frac{C_{DA}}{2C_{DB}}\left[\frac{\pi}{2}-\psi+\sin(\psi)\cos(\psi)\right] < \frac{l}{r}$$
$$\le \frac{C_{DA}}{2C_{DB}}\left[\frac{\pi-\psi+\sin(\psi)\cos(\psi)}{1+\cos(\psi)}\right] \tag{4}$$

$$\frac{l}{r} > \frac{C_{DA}}{2C_{DB}}\left[\frac{\pi-\psi+\sin(\psi)\cos(\psi)}{1+\cos(\psi)}\right] \tag{5}$$

The values of the drag factor coefficients used in these functions are reported in Fig. 4.

References

[1] F.P. Lees, Loss Prevention in the Process Industries, II Ed., Butterworth-Heinemann, Oxford, UK, 1996.

[2] CCPS, Guidelines for Chemical Process Quantitative Risk Analysis, II Ed., AIChE, New York, 2000.

[3] G.N. Pettitt, R.R. Schumacher, L.A. Seeley, Evaluating the probability of major hazardous incidents as a result of escalation event, Journal of Loss Prevention in the Process Industries 6 (1993) 37.

[4] D.F. Bagster, R.M. Pitblado, The estimation of domino incident frequencies—an approach, Process Safety and Environmental Protection 69 (1991) 196.

[5] F.I. Khan, S.A. Abbasi, Models for domino effect analysis in chemical process industries, Process Safety Progress 17 (1998) 107.

[6] J. Gledhill, I. Lines, Development of methods to assess the significance of domino effects from major hazard sites, CR Report 183, Health and Safety Executive, 1998.

[7] P.L. Holden, A.B. Reeves, Fragment hazards from failures of pressurised liquefied gas vessels, in: IchemE Symposium Series No. 93, 1985, p. 205.

[8] P. L. Holden, Assessment of missile hazards: review of incident experience relevant to major hazard plant, November 1988.

[9] CCPS, Guidelines for Evaluating the Characteristics of Vapor Cloud Explosions, Flash Fires and BLEVEs, AIChE, New York, 1994.

[10] W.E. Baker, P.A. Cox, P.S. Westine, J.J. Kulesz, R.A. Strehlow, Explosion Hazards and Evaluation, Elsevier, Amsterdam, 1983.

[11] V. Cozzani, G. Gubinelli, E. Salzano, Escalation thresholds in the assessment of domino accidental events, Journal of Hazardous Materials 129 (2006) 1–21.

[12] V. Cozzani, A. Tugnoli, E. Salzano, Prevention of Domino effect: from active and passive strategies to inherently safe design, Journal of Hazardous Materials 139 (2007) 209.

[13] V. Cozzani, S. Zanelli, An approach to the assessment of domino accidents hazard in quantitative area risk analysis, in: Proc. 10th Int. Symp. on Loss Prevention and Safety Promotion in the Process Industries, Elsevier, Amsterdam, 2001, pp. 1263–1274.

[14] V. Cozzani, E. Salzano, The quantitative assessment of domino effect caused by overpressure. Part I: probit models, Journal of Hazardous Material 107 (2004) 67.

[15] V. Cozzani, E. Salzano, The quantitative assessment of domino effect caused by overpressure. Part II: case-studies, Journal of Hazardous Material 107 (2004) 81.

[16] N.F. Scilly, J.H. Crowter, Methodology for predicting domino effects from pressure vessel, in: International Conference on Hazard Identification and Risk Analysis, Human Factors and Human Reliability in Process Safety, 1992, p. 1.

[17] U. Hauptmanns, A Monte-Carlo based procedure for treating the flight of missiles from tank explosions, Probabilistic Engineering Mechanics 16 (2001) 307.

[18] U. Hauptmanns, A procedure for analyzing the flight of missiles from explosions of cylindrical vessels, Journal of Loss Prevention in the Process Industries 14 (2001) 395.

[19] G. Gubinelli, S. Zanelli, V. Cozzani, A simplified model for the assessment of the impact probability of fragments, Journal of Hazardous Materials 116 (2004) 175.

[20] R. Pula, F.I. Khan, B. Veitch, P.R. Amyotte, A model for estimating the probability of missile impact: missiles originating from bursting horizontal cylindrical vessels, Process Safety Progress 26 (2007) 129.

[21] R.A. Westin, Summary of Ruptured Tank Cars Involved in Past Accidents, Report No. RA-01-2-7, Railroad Tank Car Safety Research and Test Project, Chicago, IL, 1971.

[22] R.A. Westin, Railroad Tank Car Safety Research and Test Project, Summary of ruptured tank cars involved in past accidents, RA-01-2-7 ADDENDUM 5/1/73, Railroad Tank Car Safety Research and Test Project, Chicago, IL,1973.

[23] V. Cozzani, G. Gubinelli, Assessment of missile hazard: identification of reference fragmentation patterns, Journal of Hazardous Materials, under review.

[24] V. Cozzani, G. Gubinelli, G. Antonioni, G. Spadoni, S. Zanelli, The Assessment of risk caused by domino effect in quantitative risk analysis, Journal of Hazardous Materials 127 (2005) 14.

[25] C.J.H. Van Den Bosh, R.A.P.M. Weterings, Methods for the Calculation of Physical Effects (Yellow Book), Committee for the Prevention of Disasters, The Hague, NL, 1997.

[26] T. Abbasi, S.A. Abbasi, The boiling liquid expanding vapour explosion (BLEVE): mechanism, consequence assessment, management, Journal of Hazardous Materials 141 (2007) 489.

[27] M.R. Baum, Failure of a horizontal pressure vessel containing a high temperature liquid: the velocity of end-cap and rocket missiles, Journal of Loss Prevention in the Process Industries 12 (1999) 137.

[28] M.R. Baum, Rupture of a gas-pressurized cylindrical vessel—the velocity of a detached end-cap, Journal of Loss Prevention in the Process Industries 8 (1995) 149.

[29] C.M. Pietersen, Analysis of the LPG disaster in Mexico City, Journal of Hazardous Materials 20 (1988) 85–107.

[30] U.S. Chemical, Safety and Hazard Investigation Board, Propane tank explosion, Investigation Report No. 98-077-I-IA, 1998.